CHALMERS
UNIVERSITY OF TECHNOLOGY

OPTIMIZED BOGIE SYSTEM DAMPING WITH RESPECT TO SAFETY AND COMFORT

In Proceedings of the 21st International Symposium
on Dynamics of Vehicles on Roads and Tracks,
IAVSD'09, 17-21 August 2009,KTH, Stockholm,Sweden.

OPTIMIZED BOGIE SYSTEM DAMPING WITH RESPECT TO SAFETY AND COMFORT

Albin Johnsson*, Viktor Berbyuk and Mikael Enelund
Department of Applied Mechanics, Chalmers University of Technology
SE 412 96 Göteborg, Sweden
*Corresponding author email: albin.johnsson@chalmers.se

Abstract

Here the lateral damping (two dampers) is optimized and investigated with respect to safety and comfort for an eight degree of freedom model of a train bogie. The train bogie model is nonlinear due to the excitations caused by the irregularities and the wheel–track interface forces. Train running at different speeds will have different optima and optimal damping parameters with respect to both comfort and safety. The aim is to optimize the dynamic behavior for a wide range of forward service speeds up to 300 km/h. A multiobjective optimization routine is used and the results are presented in terms of Pareto fronts. To optimize the behavior semi–active functional components are required. A scheme to control semi–active lateral damping components with respect to forward speed is suggested. This can significantly improve the dynamic behavior with simultaneously respect to safety and comfort. Finally, we investigate the use of two lateral damping components with the possibility to change behavior at a certain switch time. At least for some service speeds these semi-active damping components are find to be able to improve the dynamic behavior. The understanding of the influence of the design parameters is valuable in further improving the general performance of a high speed train with respect to safety and comfort.

1 INTRODUCTION

It is known that utilization of semi-active or active functional components can significantly improve the performance of ground vehicles. Development of semi-active and active suspension technologies has been ongoing for the last decades, and many promising research results have been presented, implemented, and tested, see, *e.g.*, Goodall *et al.* [2, 6, 7] and references therein. However, active suspensions are still relatively uncommon in commercial railway vehicles, mainly because of the additional cost of implementation. Studies of semi-active and active suspensions in railway vehicle dynamics, both theoretical and experimental, can be found in, *e.g.*, [12–15]. Multidisciplinary methods for optimizing the design of a railway vehicle are starting to include evolutionary optimization algorithms which are more effective than classical optimization in handling conflicting optimization problems, see *e.g.*, [8]. When considering the suspension system of a train vehicle, the main two requirements on the system are safety and comfort, which are conflicting to some extent.

Here we will investigate the possibilities to optimize the lateral damping characteristics of a train bogie with respect to safety and comfort for a wide range of service speeds in order to improve the dynamic behavior of a bogie system running on a straight track. In such systems there are upper speed limits to safely drive the vehicles without risk of derailment. We will investigate how the damping characteristics influences these limit speeds and also how the comfort is affected. The results are believed to be valuable for the design of semi-active or active functional components to be used in the bogie system and for control algorithms of such systems. Moreover, the results are also potentially useful for basic understanding of the behavior of the conventional bogie system.

An eight degree of freedom model of a conventional bogie system for a high speed train passenger coach is formulated and implemented numerically. Within the model the vibrations of the bogie system caused by excitations due to wheel-rail contact and track irregularities are calculated. For the wheel-rail contact force we use the non-linear Vermeulen-Johnson model, which is an extension of the Kalker linear theory. Objective functions for safety and comfort are formulated and discussed. Finally the biobjective optimization problem with respect to lateral damping parameters is formulated and solved using a multiobjective evolutionary optimization algorithm in Matlab.

2 MODELING OF MECHANICAL SYSTEM

Based on previous work, [4, 6, 7, 9, 10, 14], we suggest the usage of models with varying complexity in order to effectively study different stages/parts of the design procedure. It is important to study the behavior of rather simplified models, especially for introduction of control systems in order to reduce the complexibility. To derive a suitably simple bogie system model, we take the plane-view model [14] and the Cooperrider model [10] as starting points. Model parameters valid for High Speed Trains (HST) with service speeds up to 250 km/h are used.

2.1 Model of Bogie System

The present bogie system, (half vehicle model), consists of four bodies; two wheelsets, one bogie frame and one carbody, which are connected with two types of suspensions. The bogie frame is connected to the cart through the secondary suspension and the wheels are connected with the bogie frame with the primary suspension, see Figure 1.

The mathematical model of this system, *i.e.*, the equations of motions with initial states, can be written as

$$\boldsymbol{M}\ddot{\boldsymbol{q}} + \boldsymbol{C}\dot{\boldsymbol{q}} + \boldsymbol{K}\boldsymbol{q} = \boldsymbol{F}(t,\, \boldsymbol{q},\, \dot{\boldsymbol{q}}), \tag{1}$$

$$\boldsymbol{q}(0) = \boldsymbol{q}_0,\;\; \dot{\boldsymbol{q}}(0) = \dot{\boldsymbol{q}}_0, \tag{2}$$

where $\boldsymbol{q}$ is the vector of the generalized coordinates of the model, $\boldsymbol{M}$, $\boldsymbol{C}$, and $\boldsymbol{K}$ are the inertia, damping and stiffness matrices, respectively, and $\boldsymbol{F}(t,\, \boldsymbol{q},\, \dot{\boldsymbol{q}})$ is the vector of the external forces applied to the system due to excitation from the wheel-rail contact. The model has eight degrees of freedom, describing the lateral behavior of the system, assuming it is uncoupled with the vertical behavior. The following degrees of freedom are included; lateral and yaw motions for the wheelset, $(y^{\text{fw}}, \theta^{\text{fw}}, y^{\text{rw}}, \theta^{\text{rw}})$, lateral, yaw and roll motion for the bogie frame, $(y^{\text{bf}}, \theta^{\text{bf}}, \varphi^{\text{bf}})$, and lateral motion for the carbody, (y^{cb}). The nodal degree of freedom vector and the matrices in Eq. (1) then take the

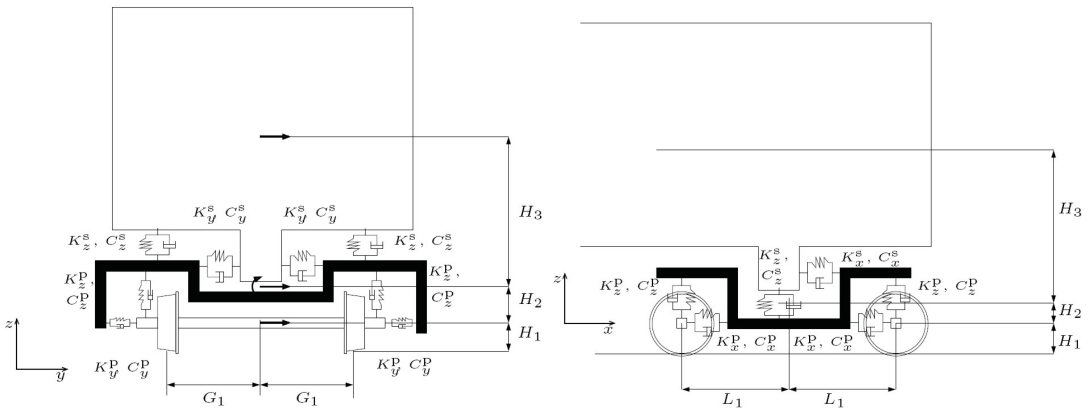

Figure 1: *The mechanical model of the bogie system.*

form

$$\boldsymbol{q} = [y^{\text{fw}}, \theta^{\text{fw}}, y^{\text{rw}}, \theta^{\text{rw}}, y^{\text{bf}}, \theta^{\text{bf}}, \varphi^{\text{bf}}, y^{\text{cb}}]^{\text{T}},$$
$$\boldsymbol{M} = \text{diag}([m^{\text{w}}, I_z^{\text{w}}, m^{\text{w}}, I_z^{\text{w}}, m^{\text{bf}}, I_z^{\text{bf}}, I_y^{\text{bf}}, m^{\text{cb}}]),$$
$$\boldsymbol{K} = \begin{bmatrix} k_{11} & 0 & 0 & 0 & k_{15} & k_{16} & k_{17} & 0 \\ 0 & k_{22} & 0 & 0 & 0 & k_{26} & 0 & 0 \\ 0 & 0 & k_{33} & 0 & k_{35} & k_{36} & k_{37} & 0 \\ 0 & 0 & 0 & k_{44} & 0 & k_{46} & 0 & 0 \\ k_{51} & 0 & k_{53} & 0 & k_{55} & k_{56} & k_{57} & k_{58} \\ k_{61} & k_{62} & k_{63} & k_{64} & k_{65} & k_{66} & k_{67} & k_{68} \\ k_{71} & 0 & k_{73} & 0 & k_{75} & k_{76} & k_{77} & k_{78} \\ 0 & 0 & 0 & 0 & k_{85} & k_{86} & k_{87} & k_{88} \end{bmatrix} \quad \text{and}$$
$$\boldsymbol{C} = \begin{bmatrix} c_{11} & 0 & 0 & 0 & c_{15} & c_{16} & c_{17} & 0 \\ 0 & 0 & 0 & 0 & 0 & 0 & 0 & 0 \\ 0 & 0 & c_{33} & 0 & c_{35} & c_{36} & c_{37} & 0 \\ 0 & 0 & 0 & 0 & 0 & 0 & 0 & 0 \\ c_{51} & 0 & c_{53} & 0 & c_{55} & c_{56} & c_{57} & c_{58} \\ c_{61} & 0 & c_{63} & 0 & c_{56} & c_{66} & c_{67} & c_{68} \\ c_{71} & 0 & c_{73} & 0 & c_{75} & c_{76} & c_{77} & c_{78} \\ 0 & 0 & 0 & 0 & c_{85} & c_{86} & c_{87} & c_{88} \end{bmatrix}.$$

All simulations have been conducted with the parameter values of the bogie system representing a railway vehicle in service, except the values for the damping parameters for the lateral primary dampers, C_y^{p}, and for the lateral secondary dampers, C_y^{s}. The parameters C_y^{p} and C_y^{s} are subjected to optimization.

2.2 Contact modeling

We adopt the non-linear creep-force contact model by Vermeulen-Johnson, which is based on Kalker's linear theory [1]. It is assumed that the contact patch is elliptic with semi-axis a and b, calculated according to the Hertz theory. The contact forces $R_{x'}$ and $R_{y'}$ are calculated from the linear counterparts

$$R_{x'}^* = -\kappa_{11}\xi_{x'}, \quad R_{y'}^* = -\kappa_{22}\xi_{x'} \tag{3}$$

where $\xi_{x'}$ and $\xi_{y'}$ are the creepage in the contact surface coordinates (x', y', z') and κ_{ij} are creep coefficients related to the semi-axis of the contact surface. The norm of the linear creep force vector is

$$R_R^* = \sqrt{(R_{x'}^*)^2 + (R_{y'}^*)^2}. \tag{4}$$

Now, the non-linear creep forces are calculated as

$$R_{x'} = R_{x'}^* \frac{R_R}{R_R^*}, \quad R_{y'} = R_{y'}^* \frac{R_R}{R_R^*}, \tag{5}$$

with

$$R_R = \begin{cases} \mu R_{z'} \left[\left(\frac{R_R^*}{\mu R_{z'}} \right) - \frac{1}{3} \left(\frac{R_R^*}{\mu R_{z'}} \right)^2 + \frac{1}{27} \left(\frac{R_R^*}{\mu R_{z'}} \right)^3 \right] & \frac{R_R^*}{\mu R_{z'}} < 3 \\ \mu R_{z'} & \frac{R_R^*}{\mu R_{z'}} \geq 3, \end{cases}$$

where $R_{z'}$ is the normal force and μ is the kinematic coefficient of friction. The creep forces in Eq. (5) are calculated for each wheel ($\boldsymbol{R}_{\text{wf}}^{\text{left}}$, $\boldsymbol{R}_{\text{wf}}^{\text{right}}$, $\boldsymbol{R}_{\text{wr}}^{\text{left}}$, $\boldsymbol{R}_{\text{wr}}^{\text{right}}$, where subindexes wf and wr stand for front wheelset and rear wheelset, respectively). Upon using this, the external force vector $\boldsymbol{F}(t,\ \boldsymbol{q},\ \dot{\boldsymbol{q}})$ in Eq. (1) is

$$\boldsymbol{F}(t,\ \boldsymbol{q},\ \dot{\boldsymbol{q}}) = \begin{bmatrix} R_{y,\text{wf}}^{\text{left}} + R_{y,\text{wf}}^{\text{right}} \\ -G_1 R_{x,\text{wf}}^{\text{left}} - G_1 \sin(\theta^{\text{wf}}) R_{y,\text{wf}}^{\text{left}} + G_1 R_{x,\text{wf}}^{\text{right}} + G_1 \sin(\theta^{\text{wf}}) R_{y,\text{wf}}^{\text{right}} \\ R_{y,\text{wr}}^{\text{left}} + R_{y,\text{wr}}^{\text{right}} \\ -G_1 R_{x,\text{wr}}^{\text{left}} - G_1 \sin(\theta^{\text{wr}}) R_{y,\text{wr}}^{\text{left}} + G_1 R_{x,\text{wr}}^{\text{right}} + G_1 \sin(\theta^{\text{wr}}) R_{y,\text{wr}}^{\text{right}} \\ 0 \\ 0 \\ 0 \\ 0 \end{bmatrix}, \tag{6}$$

were G_1 is the half gauge distances, see Figure 1.

The wheels are assumed to have a profile with constant conicity and therefore the flanges of the wheels are modeled with very stiff non-linear springs as in [9] (the expression is valid for both the front and the rear wheelset)

$$R_y^{\text{flange}} = \begin{cases} K^{\text{flange}}(\eta - y^{\text{w}}) & y^{\text{w}} > \eta \\ K^{\text{flange}}(\eta + y^{\text{w}}) & y^{\text{w}} < \eta \\ 0 & \text{otherwise,} \end{cases} \tag{7}$$

where $\eta = 9.1\,\text{mm}$ is the free zone, y^{w} is y^{fw} or y^{rw} and $K^{\text{flange}} = 14.6\,\text{MN/m}$ is the flange stiffness. This is treated as an additional contact force and is added to $\boldsymbol{F}$.

Excitations by Geometrical Track Irregularities

We study the effect of track irregularities with the use a non-linear contact model in order to account for displacements of the contact point. The irregularities are modeled with a stationary stochastic process and described by a one-sided density function as in [3]

$$\Phi(\Omega) = A\frac{\Omega_c^2}{(\Omega_r^2 + \Omega)(\Omega_c^2 + \Omega)}, \tag{8}$$

with parameter values

$$\Omega_c = 0.8246 \text{ rad/m, and } \Omega_r = 0.0206 \text{ rad/m,} \tag{9}$$

where Ω is the distribution factor and A is the scaling factor that is used to specify the level of the irregularities. We use the following values $A_{\text{low}} = 0.59233 \cdot 10^{-6}\text{m}$, $A_{\text{mid}} = 0.7930 \cdot 10^{-6}\text{m}$ and $A_{\text{high}} = 1.58610 \cdot 10^{-6}\text{m}$. A sample of the stochastic excitation profile can now be calculated with the spectral representation method as

$$\zeta_i(x) = \sqrt{2}\sum_{n=0}^{N-1} a_n \cos(\Omega_n x + \varphi_n), \tag{10}$$

where φ_n are uniformly distributed phase angles in the range $[0, 2\pi]$, $\Omega_n = n\Delta\Omega,\ \Delta\Omega = \Omega_u/N$, for $n = 0, 1, \ldots, N-1$, and Ω_u is the highest frequency while the coefficients a_n are

$$a_0 = 0, \quad a_1 = \sqrt{\left(\frac{\Phi(\Delta\Omega)}{2\pi} + \frac{\Phi(0)}{3\pi}\right)\Delta\Omega}, \quad a_2 = \sqrt{\left(\frac{\Phi(2\Delta\Omega)}{2\pi} + \frac{\Phi(0)}{12\pi}\right)\Delta\Omega}, \text{ and}$$
$$a_n = \sqrt{\frac{\Phi(\Omega_n)}{2\pi}\Delta\Omega}, \quad \text{for } n = 3, 4, \ldots, N-1.$$

A set of three samples is calculated, one for each level of irregularity, with $\Omega_u = 13.57\,\text{rad/s}$, and $N = 3540$. The subindex i specifies which level of irregularities the sample has. Here $i \in \{\text{low, mid, high}\}$. The data is then used as input to the bogie model. The displacements of the contact point for the left and right wheel are $y_{\text{r}} = y_{\text{l}} = \zeta_i(x)$, where x is the traveled distance.

2.3 First Order Formulation

We now rewrite the model to a system of first order differential equations in state space form with $\boldsymbol{x} = [\,\boldsymbol{q}^{\text{T}},\ \dot{\boldsymbol{q}}^{\text{T}}]^{\text{T}}$. Formally the governing equations can be written as

$$\dot{\boldsymbol{x}} = \boldsymbol{f}(t,\ \boldsymbol{x},\ \boldsymbol{d},\ \boldsymbol{p},\ \boldsymbol{s},\ \boldsymbol{u}, V), \quad \boldsymbol{x}(0) = \boldsymbol{x}_0, \quad t \in [t_0, t_{\text{f}}], \tag{11}$$

where $\boldsymbol{d} = [d_1, d_2]^{\text{T}} = [C_y^{\text{p}}, C_y^{\text{s}}]^T$ is the vector of design parameters, *i.e.*, the damping constants, $\boldsymbol{p} = [p_1, p_2, \ldots, p_{N_p}]$ is the vector of system structural parameters which includes the stiffens, mass, inertia parameters and the other damping parameters and $\boldsymbol{s} = [s_1, s_2, \ldots, s_{N_s}]$ is the vector of system dynamics parameters including parameters such as coefficient of friction, contact model parameters, and geometrical parameters of track and wheel while $\boldsymbol{u}(t, V) = \zeta_i(tV)$ is the vector of excitations, and V is the constant speed of the train. The initial states $\boldsymbol{x}_0$ are limited to ensure realistic conditions.

3 VIBRATION DYNAMICS OF BOGIE SYSTEM

The solution to Eq. (11) is now obtained and studied. The vehicle travels 500 m on a straight track and the structural and the dynamical parameters are taken to be constant. The initial value $\boldsymbol{x}_0$ is taken as the final state of a 1000 m run with $\boldsymbol{u}_0(t, V) = \zeta_2(tV)$, $V = 200$ km/h and $\boldsymbol{x}_0 = \mathbf{0}$. The solution is given as the dynamical response,

$$\begin{aligned} &\boldsymbol{x} = \boldsymbol{x}(t,\ \boldsymbol{x}_0,\ \boldsymbol{d}_0,\ \boldsymbol{p}_0,\ \boldsymbol{s}_0,\ \boldsymbol{u}_0(t, V), V) \quad \text{for } t \in [t_0, t_\mathrm{f}], \\ &\boldsymbol{d}_0 \in \boldsymbol{\mathcal{X}}_j, \text{ for } j \in \{1, 2\},\ \ \boldsymbol{p}_0, \text{ and } \boldsymbol{s}_0 \text{ are constant}, \\ &\boldsymbol{u}_0(t, V) = \zeta_i(tV), \text{ for } i \in \{\text{low, mid, high}\} \text{ and } V \in [150, 300] \text{ km/h}, \end{aligned} \tag{12}$$

where $\boldsymbol{\mathcal{X}}_j$ the design parameter space. In the first part of the study the design parameter space is time independent

$$\boldsymbol{\mathcal{X}}_1 = \left\{ \boldsymbol{d}(t) \,\middle|\, \boldsymbol{d}(t) = \boldsymbol{d} \in \mathbb{R}^2, t_0 \le t \le t_\mathrm{f} \right\} \tag{13}$$

and in the second part the design parameter space is piecewise time-constant

$$\boldsymbol{\mathcal{X}}_2 = \left[\boldsymbol{d}(t) \,\middle|\, \boldsymbol{d}(t) = \begin{cases} \boldsymbol{d}^1 \in \mathbb{R}^2, & t_0 \le t \le t_s \\ \boldsymbol{d}^2 \in \mathbb{R}^2, & t_s < t \le t_\mathrm{f} \end{cases} \right]. \tag{14}$$

3.1 Objectives of Safety and Comfort

In order to evaluate the performance of the bogie system the following vector of objective functions representing safety and comfort are used

$$\boldsymbol{\mathcal{F}} = [\mathcal{F}_{\text{safety}}, \mathcal{F}_{\text{comfort}}]^\mathrm{T} \tag{15}$$

to measure the properties of interest for performance of the bogie system. The safety measure $\mathcal{F}_{\text{safety}}$ relates to the forces applied on the wheels due to the wheel-rail contact, which have potential to damage both rail and wheel and to cause derailment,

$$\mathcal{F}_{\text{safety}} = \max_{t \in [t_0, t_\mathrm{f}]} \left\{ \max \left(\left| \frac{R_{y,\text{wf}}(t)}{R_{z,\text{wf}}(t)} \right|, \left| \frac{R_{y,\text{wr}}(t)}{R_{z,\text{wr}}(t)} \right| \right) \right\}. \tag{16}$$

A low value of $\mathcal{F}_{\text{safety}}$ corresponds to a high level of safety. The comfort measure $\mathcal{F}_{\text{comfort}}$ is the RMS of the acceleration of the carbody which holds the passengers

$$\mathcal{F}_{\text{comfort}} = \sqrt{\frac{1}{t_\mathrm{f} - t_0} \int_{t_0}^{t_\mathrm{f}} |\ddot{y}^{\text{cb}}(t)|^2 \mathrm{d}t}. \tag{17}$$

where t_0 is the starting time and t_f is the final time. A low value of $\mathcal{F}_{\text{comfort}}$ corresponds to a high level of comfort. The safety objective function Eq. (16) is constrained by a given maximal value, $\mathcal{F}_{\text{safety}}^{\text{limit}} = 1.15$, *i.e.*, the objective is not allowed to exceed 1.15 due to risk of derailment. The value is given by the Weinstock Limit, see [1].

3.2 Sensitivity Analysis

To investigate the possibilities for optimization of the damping constants with respect to the safety and comfort objectives in Eqs. (16) and (17), we consider the sensitivity of objectives to the forward speed and level of track irregularities as well as to the damping constants. The results are shown in Figures 2 and 3. In Figures 2a and Figure 2b the damping constants are taken as the initial values. In Figure 2a the irregularities are taken as $\boldsymbol{u}_0(t, V) = \zeta_{\text{mid}}(tV)$, while in Figure 2b the forward speed is taken as $V = 200$ km/h. In Figures 3 the irregularities are taken as $\boldsymbol{u}_0(t, V) = \zeta_{\text{mid}}(tV)$ and the forward speed is taken as $V = 200$ km/h.

As seen in Figure 2a, for speeds below 250 km/h the objectives are relatively constant and it seems as the increase of speed has only minor effects on the objectives for lower speeds, but for speeds above 250 km/h both objectives (in particular the safety objective) are significantly increased with increased speed. Some changes in the dynamical behavior have occurred as the speed input increases. One possible explanation for this is that the non-linear behavior of contact forces becomes dominant. Also, for the speeds $V > 275$ km/h the safety objective becomes larger than the given maximal value

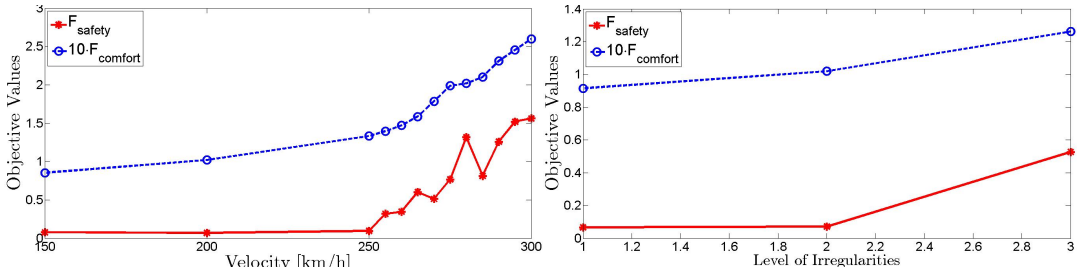

(a) (b)

Figure 2: *Left figure (a): Sensitivity of objectives* versus *forward speed* V. *Right figure (b): Sensitivity of objectives* versus *level of irregularities.*

$\mathcal{F}_{\text{safety}}^{\text{limit}}$. The safety objective is not monotonically increasing with the speed, which could have been anticipated. However, because a change in speed will shift the frequency of the irregularities we suggest that the changes of the safety objective between $V \in [270, 300]$ km/h are due to the shift of weight in excitation frequency. As seen in Figure 2b, the comfort objective is relatively independent to increased level of irregularities, while the safety objective again is constant for low irregularities and increases for the high level of irregularities. But as we only consider three different levels of irregularities it is difficult to draw any further conclusions.

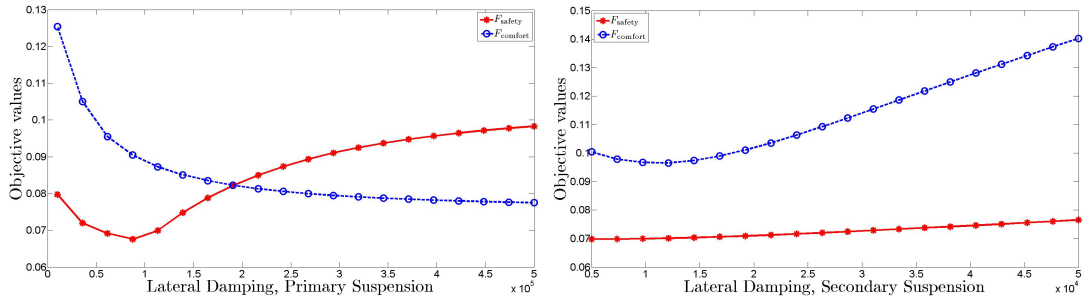

(a) (b)

Figure 3: *Left figure (a): Sensitivity of objectives* versus *the lateral primary damping constant* C_y^p *with* $C_y^s = 20$ *kNs/m. Right figure (b): Sensitivity of objectives* versus *the lateral secondary damping constant* C_y^s *with* $C_y^p = 40$ *kNs/m.*

In Figure 3a we observe that the safety objective has a minimum at approximately 60 kNs/m for the primary damping constant, while the comfort objective is decreasing with increased primary damping constant. Whereas, in Figure 3b we observe a minimum of the comfort objective at approximately 13 kNs/m for the secondary damping constant, while the safety objective is almost constant for increased secondary damping constant. As we see in Figure 3a-3b, the system is much less sensitive to changes in the damping constants than to the speed and level of irregularities. However, the damping still has impact on the system as the relative change of the safety objective is $\sim 30\%$ and for the comfort objective the relative change is $\sim 40\%$. Also, the two objectives have different minima for the damping parameters. This means that for optimal safety, there will be a certain trade off due to compromised comfort.

4 OPTIMIZATION DUE TO OBJECTIVES OF SAFETY AND COMFORT

4.1 Statement of Problem

Using the governing equation Eq. (12) and the objective functions Eqs. (15), (16) and (17) the optimization problem can be formulated as follows;

Problem 1. *It is required to determine the solution of the variational equations*

$$\mathcal{F}_i(\, \boldsymbol{x}(\, \boldsymbol{d}_{\rm opt},\, \boldsymbol{p},\, \boldsymbol{s},\, \boldsymbol{u})) = \min_{\boldsymbol{d}\, \in\, \boldsymbol{\mathcal{X}}} \mathcal{F}_i(\, \boldsymbol{x}(\, \boldsymbol{d},\, \boldsymbol{p},\, \boldsymbol{s},\, \boldsymbol{u}), \quad i = 1, 2 \tag{18}$$

subject to differential constraints

$$\dot{\boldsymbol{x}} = \boldsymbol{f}(t,\, \boldsymbol{x},\, \boldsymbol{d},\, \boldsymbol{p},\, \boldsymbol{s},\, \boldsymbol{u}, V),$$

given $\boldsymbol{p} = \boldsymbol{p}_0$, $\boldsymbol{s} = \boldsymbol{s}_0$ *and* $\boldsymbol{u} = \boldsymbol{u}_0$, *initial state* $\boldsymbol{x}(t = 0) = \boldsymbol{x}_0$ *and algebraic constraints* $\boldsymbol{d}(t) \leq [500, 500]^{\rm T}{\rm kNs/m} \quad \boldsymbol{d}(t) \geq [0, 0]^{\rm T}{\rm kNs/m}$.
Also, the safety objectives is constrained with $\mathcal{F}_{\rm safety}(\, \boldsymbol{x}(\, \boldsymbol{d}_{opt},\, \boldsymbol{p},\, \boldsymbol{s},\, \boldsymbol{u})) \leq \mathcal{F}^{\rm limit}_{\rm safety}$.

We consider two cases of Problem 1. First, Problem 1a with $\boldsymbol{\mathcal{X}} = \boldsymbol{\mathcal{X}}_1$ as in Eq. (13), were the design parameters are taken to be constant for each optimization, thus this optimization problem has two design parameters. Second, Problem 1b with $\boldsymbol{\mathcal{X}} = \boldsymbol{\mathcal{X}}_2$ as in Eq. (14), were each design parameters can switch values at a certain time, thus this optimization problem has five design parameters, two primary damping constants, two secondary damping constants and the switching time.

Problem 1 is a biobjective optimization problem, as there is two objectives to simultaneously minimize. However, if the two objectives do not have the same optimal solution, a tradeoff between them is required, this is called a conflict of the objectives. There exists several approaches to handle this conflict. The most widely used approach is to simply reformulate the problem to a single objective problem by weighting factors of the two objectives and thereafter use a classical optimization scheme in order to obtain a pre-weighted optimization. Another approach is to use a multiobjective optimization algorithm obtaining a set of Pareto optimized solutions, where the weighting are made in the postprocessing. Here we have chosen the second approach. The advantages with this approach are that we can study the set of optimized solutions rather than one optimal solution, gaining understanding of the system and freedom to chose among the optimal solutions.

4.2 Optimization Algorithm

Problem 1 can be solved using the multi-objective optimization routine `gamultiobj` in Matlab. This routine uses the genetic algorithm NSGA-II [5] for solving the following problem:

$$\min_{\boldsymbol{X}}\, \boldsymbol{F}(\, \boldsymbol{X}), \quad \text{subject to: } \boldsymbol{A}\boldsymbol{X} \leq \boldsymbol{b}, \text{ and } \boldsymbol{A}_{\rm eq}\, \boldsymbol{X} = \boldsymbol{b}_{\rm eq} \qquad \boldsymbol{B}_l \leq \boldsymbol{X} \leq \boldsymbol{B}_u, \tag{19}$$

were we for Problem 1a set $\boldsymbol{X} = [C_y^{\rm p}, C_y^{\rm s}]^{\rm T}$, $\boldsymbol{B}_l = [0, 0]^{\rm T}$ kNs/m, $\boldsymbol{B}_u = [500, 500]^{\rm T}$ kNs/m, $\boldsymbol{A} = \boldsymbol{A}_{\rm eq} = \boldsymbol{0}$ and $\boldsymbol{b} = \boldsymbol{b}_{\rm eq} = \boldsymbol{0}$. The chosen options for the algorithm are presented in Table 1. The

List of optimization options	
Population size	80
Population Initialization Range	$[\, \boldsymbol{B}_l\, \boldsymbol{B}_u]$
Tolerance on fitness value (TolFun)	$5 \cdot 10^{-4}$
Stall generation Limit (StallGenLimit)	15
The fraction on non-dominated front (ParetoFraction)	0.5
All other options is set to 'default'	$--$

Table 1: *Input for the optimization simulations.*

optimization routine ideally yields a set of non-dominated solutions in the design space. The design parameters $\boldsymbol{d}^*$ are non-dominated if $\boldsymbol{\mathcal{F}}(\, \boldsymbol{d}^*) \leq \boldsymbol{\mathcal{F}}(\, \boldsymbol{d}), \forall\, \boldsymbol{d} \in \boldsymbol{\mathcal{X}}$ with at least one strict inequality. Then $\boldsymbol{\mathcal{F}}^* = \boldsymbol{\mathcal{F}}(\, \boldsymbol{d}^*)$ is a point on the Pareto front. The optimization is performed for seven different speeds $V = [150, 200, 250, 270, 275, 280, 300]$ km/h.

4.3 Results of Optimization

Table 2 shows the result of the solution of Problem 1a in terms of intervals for the design parameters (primary and secondary damping constants) together with the extremes of the obtained Pareto fronts

for the different forward speeds. The extremes of the objectives are the values corresponding to the endpoints of the Pareto fronts, *i.e.*, $[\min \mathcal{F}_{\text{safety}}, \max \mathcal{F}_{\text{comfort}}]$ and $[\max \mathcal{F}_{\text{safety}}, \min \mathcal{F}_{\text{comfort}}]$. The Pareto fronts of Problem 1a are presented in Figure 4.

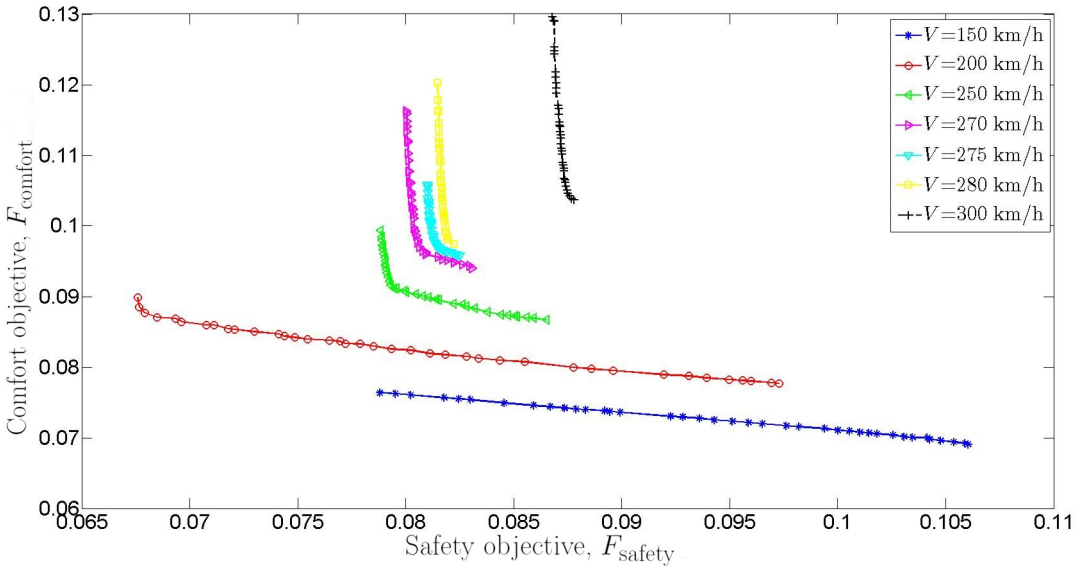

Figure 4: *Pareto fronts of the design parameters for different speeds. Each marker represents an optimum.*

As can be seen in Figure 4 the obtained fronts lie close to each other, even though the sensitivity analysis in Section 3.2 indicated that increased speed would significantly worsen the safety objective. Even though the forward speed is varied from 150 to 300 km/h, all the optimized objective values lie well within the maximal value given for the safety objective $\mathcal{F}_{\text{safety}}^{\text{limit}} = 1.15$; in fact the maximum value of $\mathcal{F}_{\text{safety}}$ is $\sim 5 - 10\%$ of the safety limit. This represent a significantly decrease compared to the safety objective function value at $\sim 150\%$ of the safety limit for the initial configuration. The change in damping constants effectively manages to raise the critical speed and thus increase the safety. This suggests that changes in damping constants can be used to avoid unwanted instabilities or non-linear behavior of the system. Also the comfort objective shows significantly improvements compared to the initial configuration. $\mathcal{F}_{\text{comfort}}$ is only increasing with $\sim 60\%$ if the speed is increased from 150 to 300 km/h compared to a corresponding increase of $\sim 200\%$ using the initial configuration.

Figure 5 illustrates how the optimized damping parameters vary for different speeds for solutions of Problem 1a. In particular we notice that in general different speeds yield different optimized damping constants. Also, the behavior of the different optimized damping parameters change with the speed. For the lower speeds the secondary damping constant is almost constant, while for the higher speeds the primary damping constant varies very little. The initial sensitivity analysis of Section 3.2 is confirmed in the sense that the optimized damper constants lie within a fairly large subset of the

Speed, [km/h]	$\boldsymbol{\mathcal{X}}_{\text{opt}}$, [kNs/m]	Extremes of the Pareto fronts, $[\min \mathcal{F}_{\text{safety}}, \max \mathcal{F}_{\text{comfort}}]$ and $[\max \mathcal{F}_{\text{safety}}, \min \mathcal{F}_{\text{comfort}}]$
150	$125 \leq C_y^{\text{p}} \leq 481,\ 21 \leq C_y^{\text{s}} \leq 25$	[0.0788, 0.0764] and [0.1060, 0.0691]
200	$102 \leq C_y^{\text{p}} \leq 450,\ 18 \leq C_y^{\text{s}} \leq 22$	[0.0676, 0.0899] and [0.0973, 0.0777]
250	$236 \leq C_y^{\text{p}} \leq 458,\ 14 \leq C_y^{\text{s}} \leq 25$	[0.0788, 0.0993] and [0.0865, 0.0867]
270	$293 \leq C_y^{\text{p}} \leq 463,\ 5 \leq C_y^{\text{s}} \leq 16$	[0.0800, 0.1162] and [0.0831, 0.0940]
275	$355 \leq C_y^{\text{p}} \leq 468,\ 9 \leq C_y^{\text{s}} \leq 17$	[0.0810, 0.1057] and [0.0830, 0.0957]
280	$403 \leq C_y^{\text{p}} \leq 477,\ 6 \leq C_y^{\text{s}} \leq 17$	[0.0815, 0.1202] and [0.0822, 0.0974]
300	$475 \leq C_y^{\text{p}} \leq 480,\ 6 \leq C_y^{\text{s}} \leq 17$	[0.0868, 0.1296] and [0.0878, 0.1037]

Table 2: *Results of optimization, Problem 1a.*

design parameter space. The effects of this is that for a semi-active device, there is a freedom to chose parameters in a large domain, but it also suggests that a large change might be needed in order to affect the system in the desired way.

Figures 6 illustrate how the behavior of the optimized objective functions for different speeds are affected by the forward speed. The optimized damping constants representing the extremes of the Pareto fronts (*i.e.*, the values corresponding to the first and last points of the Pareto fronts) are used for simulations and the safety and comfort objective *versus* speed is presented. Thus, Figures 6 can be used to formulate a simple strategy for changing the lateral damping constants in semi-active dampers with respect to forward speed. An example of optimized damping parameters for primary and secondary semi-active dampers is

$$\boldsymbol{d}_{\text{opt}}(V) = \begin{cases} [102.3; 21.9]^{\text{T}} \text{ kNs/m} & \text{for} \quad V \in [150, 225] \text{ km/h} \\ [235.7; 25.8]^{\text{T}} \text{ kNs/m} & \text{for} \quad V \in [225, 260] \text{ km/h} \\ [450.3; 18.3]^{\text{T}} \text{ kNs/m} & \text{for} \quad V \in [260, 300] \text{ km/h}. \end{cases} \tag{20}$$

This ensures that $\mathcal{F}_{\text{safety}} \leq 8\%$ of $\mathcal{F}_{\text{safety}}^{\text{limit}}$, and $\mathcal{F}_{\text{comfort}} \leq 40\%$ of the value for the initial configuration. In principal as follows from Figure 5 the optimal values of primary damping parameter increases as the speed increases.

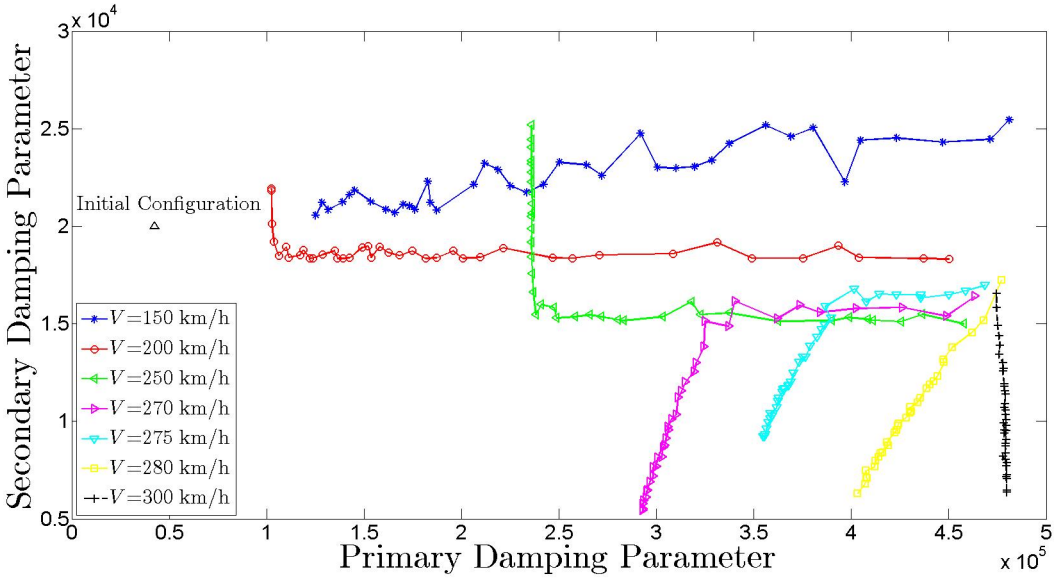

Figure 5: *Optimized damping constants for different speeds. For comparison the initial damping constants are shown.*

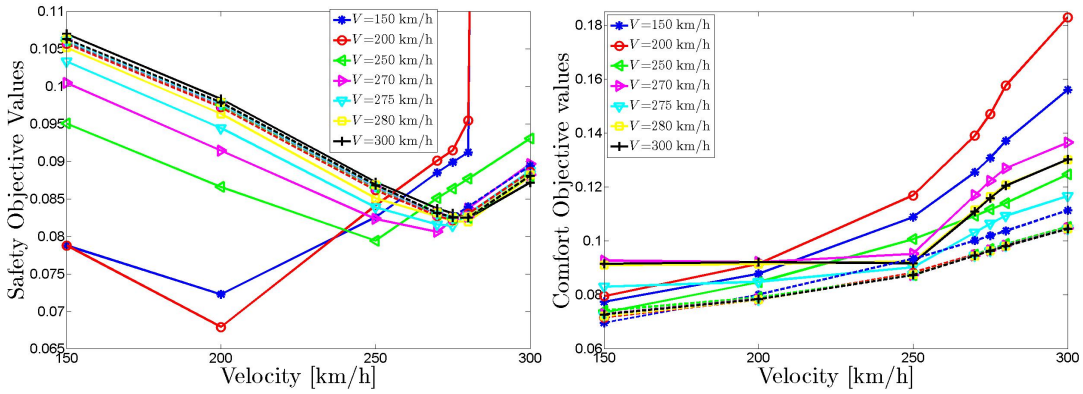

(a) (b)

Figure 6: *Left figure (a): Safety objective function* versus *speed for the extremes of the Patero fronts. Right figure (b): Comfort objective function* versus *speed for the extremes of the Patero fronts. Solid lines correspond to design parameters* $\boldsymbol{d} = \min_{\mathcal{F}_{\text{safety}}}\{\boldsymbol{\mathcal{X}}_{\mathbf{opt}}\}$ *while dashed lines correspond to design parameters* $\boldsymbol{d} = \min_{\mathcal{F}_{\text{comfort}}}\{\boldsymbol{\mathcal{X}}_{\mathbf{opt}}\}$.

Results for Problem 1b

Here we consider Problem 1b, *i.e.*, a switch time at which the design parameters can change values is introduced and the number of design parameters are increased to five. The same Matlab routine and options as in Problem 1a are used with $\boldsymbol{\mathcal{X}} = [C_y^{\text{p1}}, C_y^{\text{s1}}, t_{\text{s}}, C_y^{\text{p2}}, C_y^{\text{s2}}]^{\text{T}}$ $\boldsymbol{B}_l = [0, 0, 0.01\,\text{s}, 0, 0]^{\text{T}}$, $\boldsymbol{B}_u = [500\,\text{kNs/m}, 500\,\text{kNs/m}, t_{\text{f}}, 500\,\text{kNs/m}, 500\,\text{kNs/m}]^{\text{T}}$, $\boldsymbol{A} = \boldsymbol{A}_{\text{eq}} = \mathbf{0}$, and $\boldsymbol{b} = \boldsymbol{b}_{\text{eq}} = \mathbf{0}$. In all simulations we use the mid irregularity, and the train is running 500 m on a straight track with a forward speed in the interval $V \in [150, 300]$ km/h.

Figure 7 shows the Pareto fronts for Problem 1b. We observe that the Pareto fronts in Figure 7 are similar to the ones corresponding to Problem 1a in Figure 4. However, in Figure 7 the fronts for 150, 200 and 280 km/h are somewhat transferred to the bottom left of the plot compared to to the corresponding fronts in Figure 4, which indicate improvements in both safety and comfort.

Figure 8 shows the optimized normalized switch times, *i.e.* $t_{\text{s}}/t_{\text{f}}$, for different forward speeds *versus* the population, while Table 3 presents the min and max normalized switch times together with the optimized damping constants before and after the switching. As can be seen in Figure 8 and Table 3 the switch times are strongly dependent on forward speed. For 150 km/h the switch occurs in the very beginning, while for 270-275 km/h the switch occurs in the very end of the run, indicating that switches might be unnecessary for these speeds. On the other hand, for the rest of the speeds, the results indicate that switches might be favorable for the safety and the comfort. As seen in Figure 8 for the speed 280 km/h a second switch might be useful.

Speed, [km/h]	Normalized switching times	C_y^{p1} [kNs/m]	C_y^{s1} [kNs/m]	C_y^{p2} [kNs/m]	C_y^{s2} [kNs/m]
150	0.03-0.09	0–201.08	2.93–3.92	54.20–191.18	12.42–19.76
200	0.60-0.67	97.01–305.77	16.42–17.89	183.23–244.15	24.31–27.23
250	0.48-0.66	246.21–418.54	11.75–25.10	187.64–234.36	19.94–28.55
270	0.99-1.00	312.70–334.99	11.67–13.70	133.93–145.20	70.87–174.82
275	0.98-1.00	363.78–404.80	11.43–14.82	249.77–282.01	87.75–102.05
280	0.27-0.64	397.89–427.29	5.23–11.40	180.95–260.71	22.04–63.50
300	0.64-0.66	476.48–479.57	6.14–13.26	321.83–335.18	48.58–50.44

Table 3: *Results of optimization, Problem 1b.*

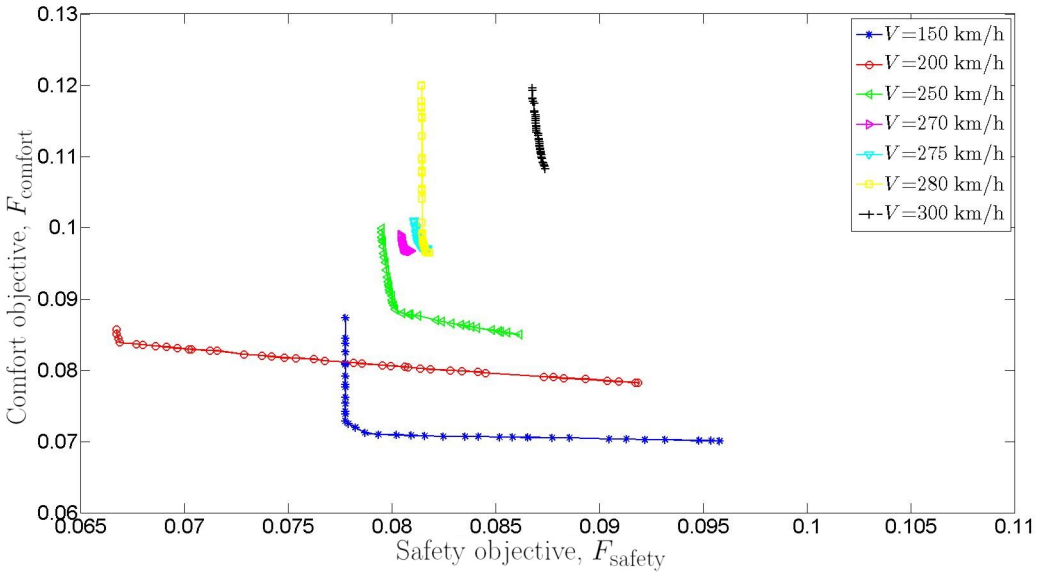

Figure 7: *Pareto fronts for Problem 1b. Each marker represents an optimum.*

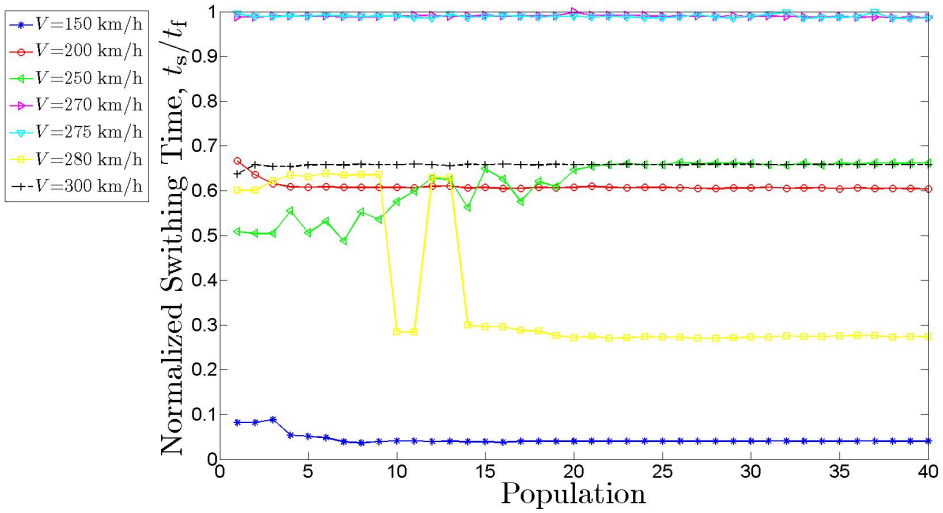

Figure 8: *Normalized switching times.*

5 CONCLUSIONS AND OUTLOOK OF FUTURE WORK

We have calculated the dynamic response and optimized the lateral damping with respect to safety and comfort for an eight degree of freedom model of a conventional train bogie. The results of the biobjective optimization are presented as Pareto fronts, see Figures 4 and 7. Compared to the initial configuration the safety objective can be decreased by approximately 90% at speeds ranging from 150 to 300 km/h. The comfort objective can be decreased by approximately 30%. We observe that the optimized secondary damping constant is almost constant while the optimized primary damping constant is dependent on forward speed. Higher speeds yield higher values of the primary damping constant, this is particulary obvious if the safety objective is in focus. We have suggested a strategy for changing damping constants with respect to forward speed.

An idea to enhance safety and comfort behavior is to introduce semi-active lateral damping components. Here we introduce dampers with one switch at which the damping constant may change values. The same switching time is imposed for both damper types. Preliminary results of the gain of this extension are disagreeing. For example, for speeds $V = 150$ and 270–275 km/h switchers seem to be superfluous, while for $V = 200$–250, 280–300 km/h switching can improve the safety and comfort. To draw any firm conclusions further investigations are needed, *e.g.*, studying parameter values and

trends which fall outside of the scope of this study and will be investigated in upcoming studies.

The introduction of semi-active components need to be further explored. For future work we also suggest further extending the design parameter space by introducing several switches. Moreover, the study of different vehicle operations, for example curving, will give a more complete picture of the possibilities to improve overall performance of a railway vehicle.

Acknowledgement

The financial support by the Ekman Family Foundation is gratefully acknowledged. The authors also would like to thank Bombardier Transportation Sweden for fruitful cooperation.

References

[1] E. Andersson, M. Berg, and S. Sitchel: *Rail Vehicle Dynamics* Universitetsservice AB, Stockholm, Sweden, 2007.

[2] S. Bruni, R. Goodall, T.X Mei, and H. Tsunashima: Control and Monitoring for railway vechicle dynamics *Vehicle System Dynamics*, Vol. 45, Nos. 7-8, July-Agust 2007, 743-779

[3] H. Claus and W. Schielen: Modeling and Simulation of Railway Bogie Structual Vibrations. *Vehicle System Dynamics Supplement*, Vol.28 , pp. 538-552 (1998).

[4] N. K. Cooperrider: The hunting behaviour of conventional railway trucks. *ASME Journal of Engineering in Industry*, 94, 1972, 752-762.

[5] K. Deb: *Multi-Objective Optimization using Evolutionary Algorithms.* John Wiley & Sons, 2001.

[6] R. Goodall: Tilting Trains and Beyond- the Future for Active Railway Suspensions - Part 1 Improving Passenger Comfort. *Computing and Control Engineering Journal* 10, 1999, 153-160.

[7] R. Goodall: Tilting Trains and Beyond- the Future for Active Railway Suspensions - Part 2 Improving Stability and Guidance. *Computing and Control Engineering Journal* 10, 1999, 221-230.

[8] Y. He and J.McPhee: Multidisciplinary Optimization of Multibody Systems with Applications to the Design of Rail Vehicles. *Multibody System Dynamics*, vol. 14, pp. 111-135, 2005.

[9] C. Nordstorøm Jensen and H. Ture: On a New Route to Chaos in Railway Dynamics. *Nonlinear Dynamics* 13, 1997, 117-129.

[10] C. Nordstorøm Jensen, M. Golubitsky and H. Ture: Symmetry, Generic Bifurcations and Mode Interaction in Nonlinear Railway Dynamics. *International Journal of Bifurcation and Chaos* 9, 7 (1999) 1321-1331.

[11] J. T. Pearson R. Goodall, T. X. Mei and G. Himmelstein : Active Stability Control Strategies for a High Speed Bogie. *Control engineering Practice* 12, 2004, 1381-1391.

[12] A. Peiffer, S. Storm, A. Röder, R. Maier and P. Frank: Active vibration control for High Speed train Bogies. *Smart Mater. Struct.* 14, 2005 1-18.

[13] D. H. Wang and W. H. Liao : Semi-Active Suspension systems for Railway Vehicles Based on Magnetorheological Fluid Dampers. *ASME 2007 International Design Engineering Technical Conferences.*

[14] A. C. Zolotas, J. T. Pearson and R. Goodall: Modelling Requirements for the design of Active Stability Control Strategies for s High Speed Bogie. *Multibody Syst. Dyn.*15, 2006, 51-66.

[15] A. Orvnäs, S. Stichel and R. Persson: On-Track Tests with Active Lateral Secondary Suspension: A Measure to Improve Ride Comfort. *ZEVrail Glasers Annalen*, Vol. 132, No. 11-12, pp. 469-477 (2008).